ELSEVIER

Materials Science and Engineering A281 (2000) 1–7

MATERIALS SCIENCE & ENGINEERING A

www.elsevier.com/locate/msea

Strain rate sensitivity of a closed-cell aluminum foam

A. Paul, U. Ramamurty *

School of Mechanical and Production Engineering, Nanyang Technological University, Nanyang Avenue 639798, Singapore

Received 9 June 1999; received in revised form 4 November 1999

Abstract

An experimental investigation into the strain rate sensitivity of a closed-cell aluminum foam at room temperature and under compression loading is conducted. The nominal strain rates are varied by four orders of magnitude, from 3.33×10^{-5} to 1.6×10^{-1} s^{-1}. Within this range, experimental results show that the plastic strength and the energy absorbed increase (by 31 and 52.5%, respectively) with increasing strain rate. However, the plastic strength was found to increase bilinearly with the logarithm of strain rate, whereas dense metals tend to show only a linear response. As is the case with dense metals, the strain rate sensitivity of the foam was not a constant value, but found to be dependent on the strain and incremental change in strain rate. These results are explained with the aid of suitable micromechanical models such as microinertial effects against the bucking of cell walls at high strain rates that are unique to foams.

Keywords: Metallic foam; Strain rate sensitivity; Energy absorption; Plastic strength

1. Introduction

Low density, cellular materials have a wide variety of applications. One class of such materials, metallic foams, offer high structural efficiency at low cost and have attracted recent attention. Potential applications of such materials include electronic component packaging, cores for structural sandwich panels, and sound and energy absorption appliances. The properties of foams can be made to vary significantly by the choice of cell wall material, the volume fraction of the solid, and the geometry of the structure. Hence, it is important to understand and model their mechanical property variation with these parameters for optimum performance. For example, recent research work, which is a consequence of the renewed interest in these materials, has addressed some of these issues. The role of cell morphology and of imperfections in governing properties such as stiffness, yield strength, crush behavior and fracture resistance, notch sensitivity, and fatigue behavior have been studied [1–12].

An area that has not yet been researched is the strain rate sensitivity of metallic foams. Such an understanding becomes imperative in applications such as crash protection or high performance packaging panels, wherein the component has to withstand high rates of deformation. Considerable amount of research has been carried out on the strain rate sensitivity of polymeric foams. It was found that while the stiffness is independent of the strain rate, the compressive yield strength increases linearly [3]. In the case of metallic foams, one can anticipate that the foam will inherently exhibit a strain rate sensitivity that is similar to the metal that it is made of. However, additional considerations such as cell wall inertia to rotation and deformation especially at high strain rates, could also play a significant role. This work has been initiated to examine these possibilities with the particular objective of developing an understanding of the effects of strain rate on plastic strength, energy absorption, and strain rate sensitivity of metallic foam.

2. Experiments

A closed-cell aluminum alloy foam material (supplied by Shinko Wire Company Ltd., Japan) with the trade name ALPORAS was used in this study. It is processed by adding about ~ 5 wt.% Ca (to enhance the viscos-

* Corresponding author. Tel.: +65-7995509; fax: +65-7911859.
E-mail address: mram@ntu.edu.sg (U. Ramamurty)

0921-5093/00/$ - see front matter
PII: S0921-5093(99)00750-9

ity) and ~3 wt.% TiH_2 particles (for foam formation) [13]. The Ti that is released from the foaming agent, as well as the Ca, remains in the Al, forming Al_4Ca and $TiAl_3$ precipitates. A macroscopic view of the material is shown in Fig. 1. Relevant properties of this material

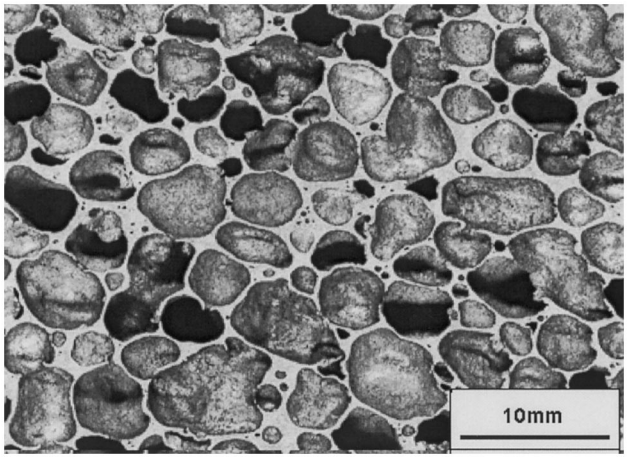

Fig. 1. Macroscopic view of the closed-cell Al foam ALPORAS.

Table 1
Relevant mechanical properties of ALPORAS

Property	Value
Relative density(ρ^*/ρ_s)	0.08–0.1
Average cell size (L)	4–5 mm
Edge thickness (t_e)	75–100 μm
Elastic modulus in tension (E_t)	0.8–1.05 GPa
Elastic modulus in compression (E_c)	0.75–1 GPa
0.2% Offset strength in tension ($\sigma_{t,0.002}$)	~1.35 MPa
0.2% Offset strength in compression ($\sigma_{c,0.002}$)	~1.28 MPa
Tensile strength (σ_t)	1.85–1.92 MPa
Compressive strength (first peak) (σ_c)	2–2.5 MPa
Fracture toughness (K_{IC})	~0.8 MPa$\sqrt{m}$

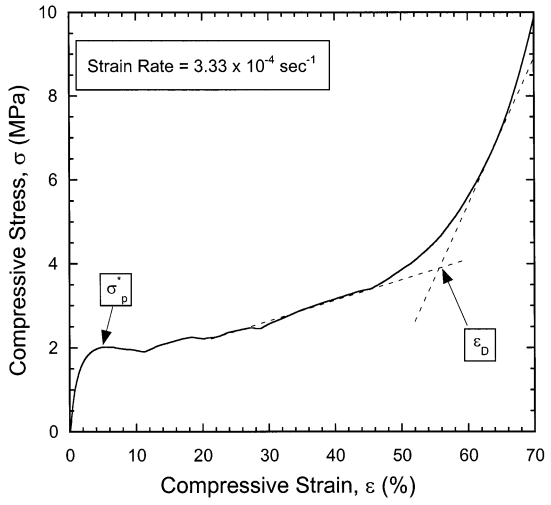

Fig. 2. Compressive stress–strain response of the ALPORAS.

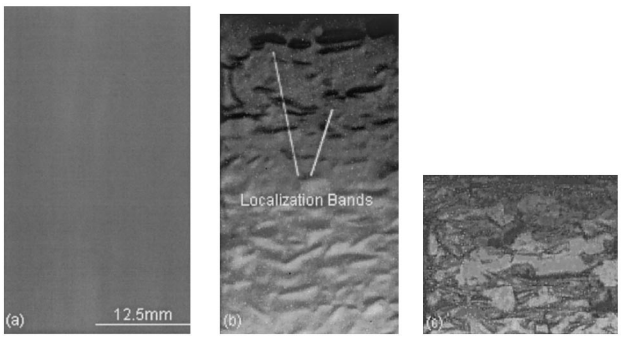

Fig. 3. Macroscopic view of the deformation bands due to strain localization at different strains. (a) No load; (b) just after σ_p^* (at ~6% strain) and (c) at the onset of densification (at ε_D, ~55% strain).

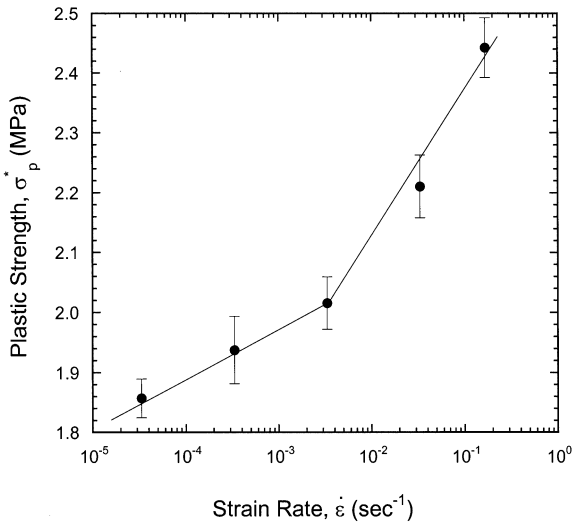

Fig. 4. Variation in the plastic strength, σ_p^*, with the nominal strain rate, $\dot{\varepsilon}$.

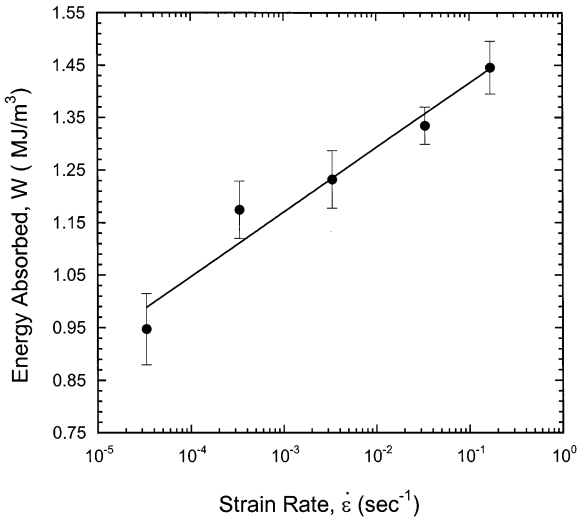

Fig. 5. Variation in the energy absorbed, W, with the nominal strain rate, $\dot{\varepsilon}$.

are listed in Table 1. Morphological features of the cells can be found in the work of Sugimura et al. [4].

Strain rate sensitivity experiments are carried out on specimens with a cross-section of 25×25 mm^2 and height of 50 mm in uniaxial compression. At least three experiments were conducted for each case. These specimens were cut carefully by electro-discharge-machining (EDM) from bigger plates. Nominal strain rates, $\dot{\varepsilon}$, (calculated on the basis of the initial specimen height and the cross-head displacement) were varied from 3.33×10^{-5} to 1.6×10^{-1} s^{-1}. The change in plastic strength, σ_p^* (defined as the first peak stress before the onset of load drop due to plastic instability), and energy absorbed per unit volume, W (defined as the area under the stress–strain curve obtained prior to the onset of densification), were measured. The latter, measured up to the onset of densification strain, ε_D, can be written as:

$$W = \int_0^{\varepsilon_D} \sigma(\varepsilon) \mathrm{d}\varepsilon \tag{1}$$

For computing W using the above relation, ε_D is taken to be 55% (see Section 3 for details).

By considering that the true flow stress, σ_t, varies with true strain rate, $\dot{\varepsilon}_t$, according to the following relation:

$$\sigma_t \propto (\dot{\varepsilon}_t)^m \tag{2}$$

and noting that $\dot{\varepsilon}_t = \dot{\varepsilon}/1 + \varepsilon$, the strain rate sensitivity, m, at a specific nominal strain ε can be computed using the following relation:

$$m = \left(\frac{\partial \log \sigma_t}{\partial \log \dot{\varepsilon}_t}\right) = \frac{\log(\sigma_{2t}/\sigma_{1t})}{\log(\dot{\varepsilon}_2/\dot{\varepsilon}_1)} \tag{3}$$

where σ_{1t} and σ_{2t} are true stresses at strain rates $\dot{\varepsilon}_1$ and $\dot{\varepsilon}_2$, respectively for a prescribed value of ε. Thus, m was measured by precipitously decreasing the strain rate either by a factor of 10 (from a strain rate of 3.33×10^{-4} to 3.33×10^{-5} s^{-1}) or 100 (from 3.33×10^{-3} to 3.33×10^{-5} s^{-1}) in the plastic flow region before the first peak stress (σ_p^*).

According to the Cottrell–Stokes law [14], m is a material property and should be a constant for a given material. However, recent work by Stüwe and Les [15], Blaz and Evangelista [16] shows that this is not necessarily the case. Their experimental results on pure Al and heat-treated Al–Mg–Si alloy show that the experimentally measured value of m will depend on the strain at which strain rates are changed. In keeping with these observations, experiments were carried out to evaluate the effect of prescribed strain on the strain rate sensitivity of ALPORAS.

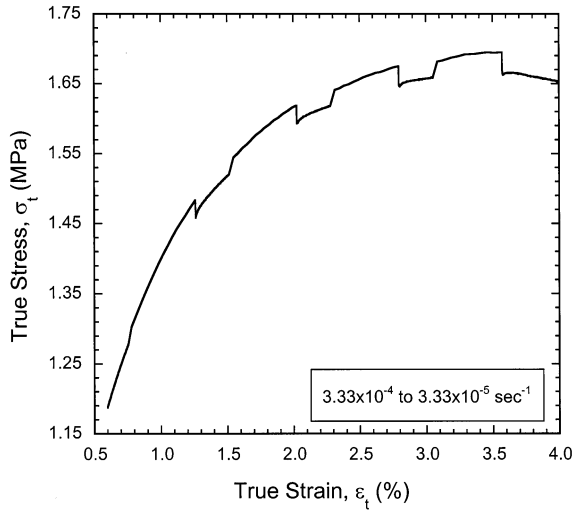

Fig. 6. Changes in true stress, σ_t, after change in strain rate, $\dot{\varepsilon}$, by a factor of 10 at different true strains.

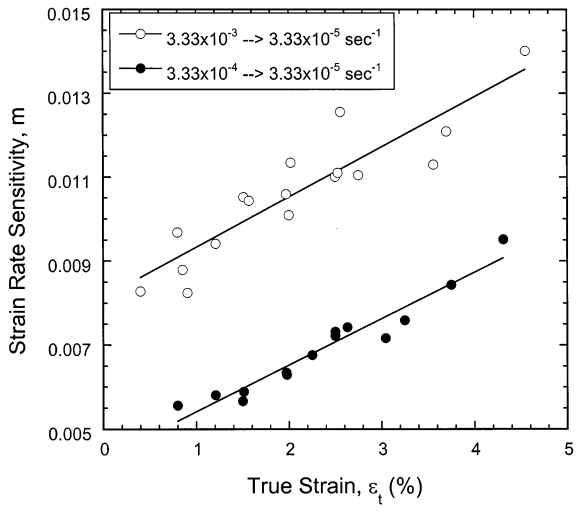

Fig. 7. A plot showing the increase in strain rate sensitivity, m, with true strain, ε_t, and strain rates.

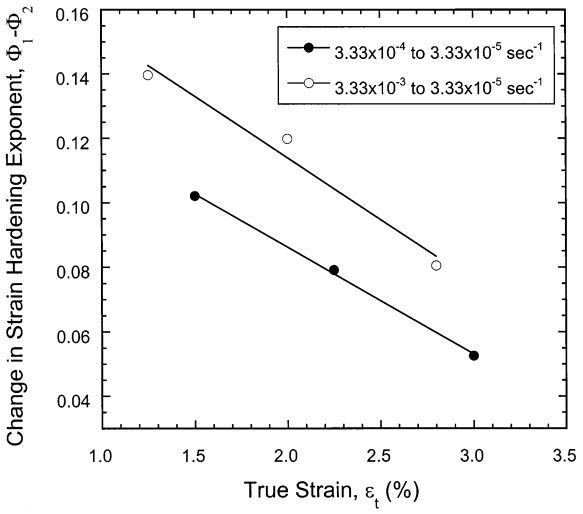

Fig. 8. Changes in the strain hardening exponent, Φ, with the strain rate, $\dot{\varepsilon}$, at different strains.

Because of the relatively large cell size, monitoring the deformation mechanisms and strain distribution in foams becomes complicated (and sometimes impossible) with conventional techniques. Bart-Smith et al. [5] have used a sophisticated technique such as the X-ray tomography to overcome this problem. However, a much simpler technique to monitor the macrostrain distribution has been developed in this work. Aluminum foil (that is commonly used in kitchens to store food etc.) was attached to the specimen using an adhesive prior to testing. The specimen is then monitored while being tested with the aid of a CCD camera. Because the foam and the foil are made of almost the same materials, their deformation characteristics will be similar. Hence, the macroscopic deformation features of the foam will be clearly reflected in the foil (because it is flat to start with and continuous). These features are digitized and recorded on a computer attached to the camera at various intervals of loading.

3. Results

A typical stress–strain curve obtained on an unnotched specimen is shown in Fig. 2. As seen from this figure, the stress–strain response of the aluminum foam exhibits three distinct regimes; a linear elastic regime at very low stresses, followed by a long stress–strain plateau wherein localized plastic collapse propagates from one cell band to another. The initiation of the first cell band collapse is reflected by the first peak in strength designated by σ_{p}^{*}. Eventually, when all the bands collapse, densification of the foam begins. This third regime in the stress strain response manifests in truncation of the plateau region and a rapid rise in stress with further strain.

The macrographs that feature the aforementioned deformation regimes in ALPORAS are shown in Fig. 3. Fig. 3(a) shows the specimen before any load is applied whereas Fig. 3(b) shows deformation pattern after the plastic collapse (at a strain of $\sim 6\%$). From Fig. 3(b), the propagation of strain localization from one band to another can be seen. Fig. 3(c) shows the deformation at onset of densification (at $\sim 55\%$ strain).

Fig. 4 shows the variation of plastic strength, σ_{p}^{*}, with the strain rate, $\dot{\varepsilon}$, (the latter plotted on a logarithmic scale as per the convention) at ambient temperature. It can be seen from this figure that the strength increases bilinearly with the $\log(\dot{\varepsilon})$, increasing relatively slowly for strain rates lower than $3.33 \times 10^{-3}\ \mathrm{s}^{-1}$, and increasing at a rapid rate at higher strain rates. The energy absorbed during plastic deformation of the foam, W, is plotted against the $\log(\dot{\varepsilon})$ in Fig. 5. Unlike the plastic strength, the energy absorbed increases linearly with increasing $\log(\dot{\varepsilon})$ throughout the strain rate range investigated in this work.

Fig. 6 shows the change in stress due to change in strain rate from 3.33×10^{-4} to $3.33 \times 10^{-5}\ \mathrm{s}^{-1}$ at different strains within the plastic collapse regime. It is clear from the figure that for the same factor (of 10) of drop in strain rate, drop in stress increases with strain, which leads to an increase in the value of m obtained. Fig. 7 shows the variation in m with strain for two different factors of strain rate change. Strain rate sensitivity was calculated by taking the flow stress just before the strain rate change and the flow stress recorded immediately after the decrease of strain rate. The seemingly large scatter in this plot arises due to the fact that several specimens were used to construct each curve. Note that if a single specimen is used, a smooth and continuous increase in m with strain will be observed. However, extracting m values from one specimen was not possible in this particular case because true strain corresponding to the first peak is small ($< 5\%$) and hence one can take only two or three points from each experiment. Therefore, several specimens are used, resulting in the scatter that arises from the specimen-to-specimen variability in mechanical properties.

Experimental results plotted in Fig. 7 show that the value of m ranges between 0.005 and 0.015. These results are consistent with the measurements of m for Al reported in literature [15,16]. It is seen from Fig. 7 that for a given amount of strain rate change, the measured value of m increases linearly with increasing strain at which the strain rates are changed. Furthermore, for any given strain, the higher the strain rate drop, the higher will be the measured m value.

4. Discussion

4.1. Variation of σ_p^* with the strain rate

The plastic stress of a closed-cell Al foam can be related to its relative density, $\rho^{*}/\rho_{\mathrm{s}}$, according to the following equation, derived using finite element analysis [11,17]:

$$\frac{\sigma_{\mathrm{p}}^{*}}{\sigma_{\mathrm{ys}}} = 0.3\left(\frac{\rho^{*}}{\rho_{\mathrm{s}}}\right) \tag{4}$$

where ρ^{*}, σ_{p}^{*} are the density and plastic collapse strength of foam and ρ_{s}, σ_{ys} are density and yield strength of solid wall material, respectively. Eq. (4) was developed assuming uniform thickness within the cell edges and the faces [11]. Compression testing of various closed-cell aluminum alloys has revealed that their plastic strength is two to ten times lower than that predicted by Eq. (4) [3]. It was argued that this discrepancy is primarily due to morphological defects, particularly non-planarities in the walls such as curves and wiggles which make the process of cell wall buckling easier [11].

With increasing strain rate, the yield strength of ductile metals such as aluminum increases slightly according to the following relation [3]:

$$\sigma^*_{ys} = (\sigma^*_{ys})^0\left(1 - \frac{A\,T}{T_m}\ln\frac{\dot{\varepsilon}_0}{\dot{\varepsilon}}\right) \quad (5)$$

where $(\sigma^*_{ys})^0$ is the yield strength of the metal at 0 K, A and $\dot{\varepsilon}_0$ are material properties, and T_m is its melting point. Because σ^*_p of a foam is directly proportional to the yield strength, σ_{ys}, of the solid from which it is made (Eq. (4)), σ^*_p should also increase linearly with $\log(\dot{\varepsilon})$. However, our experimental results show a bilinear increase in σ^*_p with the $\log(\dot{\varepsilon})$, with a transition at a strain rate of $\sim 3.33 \times 10^{-3}$ s^{-1}. This observation suggests that the mechanisms of deformation in foams may be different at different strain rate regimes. A possible explanation for this is offered in the following.

During the compression loading of a closed-cell foam, strain tends to localize into a thin band which causes buckling of cell walls and stretching of faces [3]. Localization of strain leads to a much larger local strain rate within the thin band than the apparent nominal strain rate. Typically, crushing initiates in a single band that is in contact with the loading surface and proceeds one layer after the other. This was also observed in our experiments (Fig. 3b). According to the microinertial hardening theory proposed by Klintworth and Stronge [18], at low strain rates, microinertia has very little effect, and the buckling of cell walls, which is the usual mechanism of deformation in foams, dominates. However, at very high strain rates, buckling is resisted by the inertia of the cell walls. This microinertia increases the plastic strength and tends to diffuse the localization.

Experiments conducted by Klintworth and Stronge [18] on Al honeycombs confirmed the theory of microinertial enhancement in plastic strength. For the closed-cell Al foams investigated in the current work, it is thought that such a mechanism is the reason for the observed steep increase the plastic strength at higher strain rates. However, the microinertial effects become significant at a *nominal* strain rate of ~ 0.01 s^{-1} for the ALPORAS (Fig. 4) as compared to the *local* strain rate of ~ 10 s^{-1} for the aluminum honeycomb (with a cell size of 5 mm) reported by Klintworth and Stronge [18]. An approximate estimation of the local strain rate in ALPORAS can be made by assuming that all the plastic strain is confined to a thin section whose thickness is equivalent to cell size. This is a reasonable assumption because of the localization phenomenon (discussed in the preceding paragraph). Even after accounting for such, there remains a difference of two orders of magnitude in strain rates where the microinertia becomes significant in closed-cell foams and honeycombs. This, despite similar cell sizes, is a noteworthy observation and further experimental and theoretical research is necessary to rationalize it.

4.2. Variation of W with strain rate

Experimental data for the densification strain, ε_D, for a number of polymeric foams were found to be well described by the following equation [3]:

$$\varepsilon_D = 1 - 1.4\left(\frac{\rho^*}{\rho_s}\right) \quad (6)$$

The densification strain for the ALPORAS, computed using Eq. (5), is $\sim 86\%$, significantly higher than the 55% that is used in this work for estimating the W. Note that the definition of ε_D assumes an idealized stress–strain response for the foams, which clearly demarcates the nominally constant stress plateau regime and the densification regime. In such a case, ε_D is defined as the strain at which slope of the tangent to the stress–strain curve tends to E_s, the elastic modulus of the parent metal (see for example, Fig. 1 in Ref. [17]). However, in reality, precise identification of ε_D is difficult because of the fact that there is no abrupt transition between different deformation regimes (Fig. 2). To overcome this problem, in this work ε_D was defined as the *onset of densification* and taken to be the intersection of tangents to the stress–strain curve for the cell wall collapse regime and densification regime. The ε_D was extracted from several different specimen data and the average value of such data, 55%, was fixed for computing the W for all specimens. It is interesting to note that Mukai et al. [19] use the same value for computing the energy absorption in a similar ALPORAS material.

When the foam is loaded, work is done by the forces applied to it in plastically deforming it. The work per unit volume in deforming the foam to a strain ε is simply the area under the stress strain curve up to a certain strain ε. Very little energy is absorbed in the short, linear elastic regime as shown in Fig. 2. The long plateau of the stress–strain curve arises due to bending of cell walls and stretching of cell faces, followed by cell collapse due to buckling and yielding. These mechanisms allow for large energy absorption at constant or slightly increasing stress.

In this study, energy absorption at different strain rates was measured up to the strain for onset of densification, ε_D. Because the plateau strength increases with increasing strain rate, W also increases with the strain rate because of an increase in area under the σ–ε curve. However, the W vs. $\log(\dot{\varepsilon})$ plot (Fig. 5) does not exhibit the same bilinearity shown by the σ^*_p vs. $\log(\dot{\varepsilon})$ plot (Fig. 4). A possible reason for this discrepancy may be the fact that the microinertia is effective only during the initial phase of the stress–strain curve, i.e. they only enhance the σ^*_p significantly at higher strain rates. This

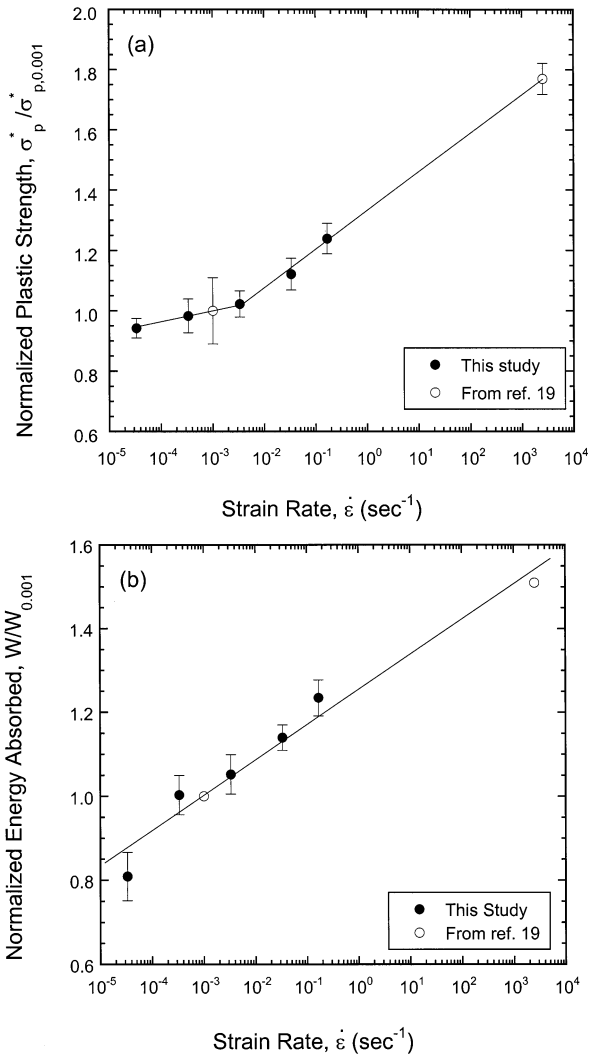

Fig. 9. Comparison of quasi-static and dynamic mechanical testing results. Variation in (a) the plastic strength, σ^*_p, and (b) the energy absorbed, W, with the nominal strain rate, $\dot{\varepsilon}$. The σ^*_p and the W are normalized with the respective properties measured at a strain rate of 1.0×10^{-3} s^{-1}.

was an observation made by Stronge and Shim [20] who have conducted dynamic crushing experiments on tightly packed arrays of thin-walled metal tubes. Microinertial effects also tend to diffuse the strain localization, making the plateau strength and in turn the overall energy absorbed increase more uniformly, as suggested by Klintworth and Stronge [18].

4.3. Strain rate sensitivity

The measured value of m, in the range of 0.005–0.015, indicates that the strain rate sensitivity in metallic foam under study arises primarily because of the processes associated with the thermal activation of dislocation glide [15]. The slope of the strain rate sensitivity plot with true strain, $dm/d\varepsilon \sim 0.12$ is also similar to that reported for Al at room temperature [16]. These observations suggest that the metallic foams essentially inherit the same strain rate sensitivity characteristics of the parent metal. However, there may be subtle differences in the mechanisms responsible.

The increase in m with strain in metallic foam can be due to two different mechanisms. Firstly during compression of metallic foam, as discussed earlier, localization of deformation into a thin band leads to a local strain rate much larger than the apparent nominal strain rate. Because the stress–strain gradient of the material in this band decreases rapidly, as manifested in the nominal yielding point to first peak stress on the stress–strain curve (Fig. 2), the strain hardening coefficient, Φ, of the material decreases rapidly from a high value to a low value. The effective strain hardening results from a balance between the strain-dependent hardening mechanisms and the time-dependent softening mechanisms [15], so that:

$$\Phi = \frac{d\sigma}{d\varepsilon} \approx \left(\frac{\partial \sqrt{\bar{\rho}}}{\partial \varepsilon} + \frac{\partial \sqrt{\bar{\rho}}}{\partial t} \frac{1}{\dot{\varepsilon}} \right) A\, G\, b \tag{7}$$

where b is a Burgers vector, $\bar{\rho}$ is the average dislocation density, G is the Gibb's free energy and A is a frequency factor. Eq. (7) shows that Φ is a function of the strain rate at any given strain. Results of Stüwe and Les [15] show that the contribution of time-dependent softening ($\partial \sqrt{\bar{\rho}}/\partial t$) increases with strain.

Secondly, microinertia associated with rotation and lateral motion of cell walls when they buckle may cause a change in strain hardening exponent with change in strain rate. Microinertia tends to suppress the more compliant buckling modes so as to increase the plastic strength and slope of the stress–strain curve [17,20].

Both the micromechanisms described above cause a decrease in Φ due to decrease in strain rate at a given strain. Fig. 8 shows a linear decrease in the relative change in Φ at different strains due to a drop in the strain rate. It also shows that for a given strain, higher the strain rate jump, higher will be the change in Φ. These observations explain the increases in strain rate sensitivity with strain rate and strain.

4.4. Comparison with the dynamic loading results

Finally, we compare the experimental results obtained in this study under quasi-static loading to those recently reported by Mukai et al. [19] under dynamic loading. The purpose of this exercise is to examine whether the strain rate sensitivity trends observed in this study on ALPORAS can be extrapolated to very high strain rates. Mukai et al. [19] have conducted experiments on ALPORAS of relative density that is similar to that used in the present work, which facilitates for a direct comparison of the data. However, their material's average cell diameter ($\sim$2.6 mm) is significantly smaller than that of the material used in this study. Possibly because of this and other mi-

crostructural differences, the average σ_p^* and W measured by Mukai et al. [19] at a quasi-static strain rate of 1.0×10^{-3} s^{-1} are relatively smaller than those measured in this work at a comparable strain rate. To overcome this disparity, the comparison is made on the basis of the normalized data.

Fig. 9(a) shows the plastic strength, σ_p^*, (normalized with the plastic strength measured at a strain rate of 1.0×10^{-3} s^{-1}, $\sigma_{p,0.001}^*$) as a function of the strain rate, $\dot{\varepsilon}$. It is seen that the σ_p^* measured under dynamic loading conditions is in reasonable agreement with the extrapolation of quasi-static results. The bilinearity observed in the variation of σ_p^* with the log($\dot{\varepsilon}$) also appears to hold well. The energy absorbed, W, (normalized with the W measured at a strain rate of 1.0×10^{-3} s^{-1}, $W_{0.001}$) is shown Fig. 9(b). An excellent linear relationship between W and the log($\dot{\varepsilon}$) through a $\dot{\varepsilon}$ range spanning eight orders of magnitude is noteworthy. Both W and σ_p^* increase approximately by 87% over this $\dot{\varepsilon}$ range. These observations suggest that properties of metallic foams are highly sensitive to the strain rate, and such sensitivity can perhaps be exploited in applications involving the foams.

5. Concluding remarks

The experiments carried out in this work show that the strain rate sensitivity characteristics of Al foam are similar to those of dense Al at room temperature. These include the similarity in the measured value of m and its dependence on the strain at which it is measured. However, there are some features, such as the bilinear increase in the plastic strength with the log($\dot{\varepsilon}$), that are distinct for the foam material. Because the buckling of cell walls is the dominant micromechanism of deformation in these foams, microinertial effects are thought to be the cause for the observed bilinearity.

The energy absorbed during plastic deformation of the ALPORAS increases (within the range of strain rates investigated) by $\sim 50\%$ with increasing strain rate. This is an important observation for applications wherein the metallic foams are used primarily for their impact energy absorption capabilities. It shows that the foam can absorb significantly high energies at high strain rates and hence will be very useful in protection against impact wherein strain rates tend to be high. This observation is also pertinent to those cases where foams may experience localized loading (such as protection against high velocity penetrants). In metallic foams, the plastic collapse is not constrained by the local surroundings, and lateral spreading is limited. Hence, their uniaxial compression results are similar to those under indentation [21].

Acknowledgements

The authors wish to express their gratitude to Prof. W.J. Stronge of Cambridge University for many useful discussions they had with him on the high strain rate behavior of cellular materials and structures.

References

[1] P.M. Weaver, M.F. Ashby, Prog. Mater. Sci. 41 (1997) 61.
[2] S.K. Maiti, L.J. Gibson, M.F. Ashby, Acta Mater. 12 (1984) 1963.
[3] L.J. Gibson, M.F. Ashby, Cellular Solids: Structure and Properties, Second ed., Cambridge University Press, Cambridge, UK, 1997.
[4] Y. Sugimura, J. Meyer, M.Y. He, H. Bart-Smith, J. Grenestedt, A.G. Evans, Acta Mater. 45 (1997) 5245.
[5] H. Bart-Smith, A.F. Bastawros, D.R. Mumm, A.G. Evans, D.J. Sypeck, H.N.G. Wadley, Acta Mater. 46 (1997) 3583.
[6] A. Paul, T. Seshacharyulu, U. Ramamurty, Scripta Mater. 40 (1999) 809.
[7] A.E. Simone, L.J. Gibson, Acta Mater. 46 (1998) 3109.
[8] A.E. Simone, L.J. Gibson, Acta Mater. 46 (1998) 2139.
[9] J.Y. Chen, Y. Huang, M. Ortiz, J. Mech. Phys. Solids 46 (1998) 789.
[10] H.X. Zhu, N.J. Mills, J.F. Knott, J. Mech. Phys. Solids 45 (1997) 1875.
[11] J. Grenestedt, J. Mech. Phys. Solids 46 (1998) 29.
[12] S. Santosa, T. Wierzbick, J. Mech. Phys. Solids 46 (1998) 645.
[13] S. Akiyama, U.S. Patent No. 4713277, 1987.
[14] A.H. Cottrell, R.J. Stokes, Proc. R. Soc. A233 (1955) 17.
[15] H.P. Stüwe, P. Les, Acta Mater. 46 (1998) 6375.
[16] L. Blaz, E. Evangelista, Mater. Sci. Eng. A207 (1996) 195.
[17] A.G. Evans, J.W. Hutchinson, M.F. Ashby, Prog. Mater. Sci. 43 (1999) 171.
[18] J.W. Klintworth, W.J. Stronge, Int. J. Mech. Sci. 30 (1988) 273.
[19] T. Mukai, H. Kanahashi, T. Miyoshi, M. Mabuchi, T.G. Neig, K. Higashi, Scripta Mater. 40 (1999) 921.
[20] W.J. Stronge, V.P.-W. Shim, Int. J. Mech. Sci. 29 (1987) 381.
[21] L.J. Gibson, M.F. Ashby, Proc. R. Soc. A382 (1982) 43.